Despeckling Polarimetric SAR Data Using a Multistream Complex-Valued Fully Convolutional Network

Mullissa, Adugna G.; Persello, Claudio; Reiche, Johannes

Despeckling Polarimetric SAR Data Using a Multistream Complex-Valued Fully Convolutional Network

Adugna G. Mullissa[ID], *Member, IEEE*, Claudio Persello[ID], *Senior Member, IEEE*, and Johannes Reiche[ID]

Abstract—A polarimetric synthetic aperture radar (PolSAR) sensor is able to collect images in different polarization states, making it a rich source of information for target characterization. PolSAR images are inherently affected by speckle. Therefore, before deriving *ad hoc* products from the data, the polarimetric covariance matrix needs to be estimated by reducing speckle. In recent years, deep learning-based despeckling methods have started to evolve from single-channel SAR images to PolSAR images. To this aim, deep learning-based approaches separate the real and imaginary components of the complex-valued covariance matrix and use them as independent channels in standard convolutional neural networks (CNNs). However, this approach neglects the mathematical relationship that exists between the real and imaginary components, resulting in suboptimal output. Here, we propose a multistream complex-valued fully convolutional network (FCN) (CV-deSpeckNet[1]) to reduce speckle and effectively estimate the PolSAR covariance matrix. To evaluate the performance of CV-deSpeckNet, we used Sentinel-1 dual polarimetric SAR images to compare against its real-valued counterpart that separates the real and imaginary parts of the complex covariance matrix. CV-deSpeckNet was also compared against the state of the art PolSAR despeckling methods. The results show that CV-deSpeckNet was able to be trained with a fewer number of samples, has a higher generalization capability, and resulted in higher accuracy than its real-valued counterpart and state-of-the-art PolSAR despeckling methods. These results showcase the potential of complex-valued deep learning for PolSAR despeckling.

Index Terms—Complex-valued, convolutional neural network (CNN), deep learning, polarimetric SAR (PolSAR), speckle.

I. INTRODUCTION

THE advent of freely available multiple polarization SAR images, such as Sentinel-1 dual polarimetric SAR (PolSAR) images, has been a game-changer for all-weather day/night geospatial applications. However, the exploitation of these data sets is complicated by the presence of speckle. Speckle is the effect that occurs from the interference of backscattered signals from multiple individual scatterers within a resolution cell. In polarimetric SAR, due to the presence of speckle, the main interest is not in the scattering matrix itself, but the estimated covariance matrix determines the randomness of the acquired SAR data vector. The covariance matrix defines the polarimetric properties of the image and has to be estimated first to derive *ad hoc* products, such as target decomposition and terrain classification [1].

Most polarimetric covariance matrix estimation methods proposed in the literature focus on spatially adaptive filters defined in a neighborhood window [1], [2]. Therefore, the main challenge is selecting which pixels to average together and how to assign the weight to each pixel. Blind low-pass filters, such as the boxcar filters, are ineffective in preserving resolution, edges, and point scatterers in the PolSAR data. Lee *et al.* [1] improved these drawbacks by minimizing the mean square error of the trace of the covariance matrix in a series of edge-aligned windows to filter elements of the covariance matrix. In [3] and [4], the scattering mechanisms are determined on a pixel-to-pixel basis to establish similarity. Lee and Pottier [5] addressed the bias issue observed with previous filters by redefining the range based on a speckle probability function. Deladalle *et al.* [6] used a nonlocal means approach to accurately estimate the covariance matrix in a heterogeneous medium without losing resolution. Recently, Deledalle *et al.* [7] used a homomorphic approach to convert the PolSAR signal to an additive noise model that embeds a Gaussian denoiser to effectively filter speckle and estimate PolSAR covariance matrix in a heterogeneous medium.

Recently, deep learning-based single-polarization SAR image despeckling techniques have gained attention [8], [9]. These methods operate by feeding pairs of noisy and clean images in the deep learning network so that the network learns a nonlinear function to transform the noisy input images to the filtered output. Deep learning-based polarimetric covariance matrix estimation is understudied compared to the single-channel SAR despeckling, and only a few studies applied convolutional neural network (CNN) to despeckle PolSAR data. Pan *et al.* [10] used a pretrained Gaussian denoising network to filter fully polarimetric SAR data and reported promising results. However, these methods did not consider the complex-valued nature of the covariance matrix. They separated the real and imaginary parts of the off-diagonal

[1]https://github.com/adugnag/CV-deSpeckNet

elements of the covariance matrix as real channels, thereby neglecting the mathematical relationship that existed between them.

To overcome these limitations and learn a more robust feature representation, complex-valued neural networks offer a potential solution. Initial works on complex-valued neural networks focused on leveraging the properties of complex numbers to learn a more robust transformation functions than real-valued networks [11], [12]. However, these networks provided the theoretical basis for complex-valued neural networks and did not see many real-world applications. Recent complex-valued deep learning frameworks focused on replicating the success of real-valued CNN. Therefore, these networks maintained the standard deep neural network architecture but redesigned the building blocks to accommodate complex-valued data tensors [13]. In the PolSAR domain, these types of complex-valued CNNs were applied to accurately classify polarimetric SAR images [14], [15]. To the best of our knowledge, the application of a complex-valued deep neural network for despeckling PolSAR data is yet to be demonstrated. In this letter, we propose for the first time a new architecture named CV-deSpeckNet that is designed to estimate a dual polarimetric covariance matrix in the complex domain.

II. METHOD

A. SAR Polarimetry

A data vector in fully polarimetric SAR sensors assuming reciprocity is given as follows: $k = (1/(2)^{1/2})[\, S_{YY} + S_{XX} \;\; S_{YY} - S_{XX} \;\; 2S_{XY} \,]^T$, where T designates a vector transpose. In dual polarimetric data as in Sentinel-1 configuration (VV VH), k reduces to $k = [\, S_{XX} \;\; 2S_{XY} \,]^T$, where the complex scattering coefficient S_{XY} indexed as $X, Y = (V, H)$ represents the vertical (V) and horizontal (H) polarization states [16]. In a distributed medium, k follows a zero mean multivariate complex circular Gaussian probability density function (pdf) given as:

$$p(k) = \frac{1}{\pi^3 |C|} \exp(-k^\dagger C^{-1} k) \tag{1}$$

which is insufficient to describe the scattering process of the scene. Therefore, the second-order statistics represented by the covariance matrix C that define the pdf of k is estimated to describe the scattering process. Here, C is given as $C = E\{kk^\dagger\}$, where $E\{\}$ is the expectation operator, $|C|$ is the determinant of C, and $\dagger$ is the matrix conjugate transpose. Here, C is an unknown deterministic quantity that has to be estimated from the data and follows a complex Wishart distribution [5]. In the PolSAR speckle filtering literature, the expectation operator is replaced by spatially adaptive filters assuming stationarity and ergodicity within the selected pixels.

The observed covariance matrix $\hat{C}$ follows a multiplicative noise model, i.e., $\hat{C} = C^{1/2} N C^{1/2}$, where N is a random speckle. The signal-dependent multiplicative noise can be converted to a signal-independent additive noise by taking the matrix logarithm of $\hat{C}$. The signal-independent model can be converted back to its original multiplicative form by taking the matrix exponent. In this letter, we apply a complex-
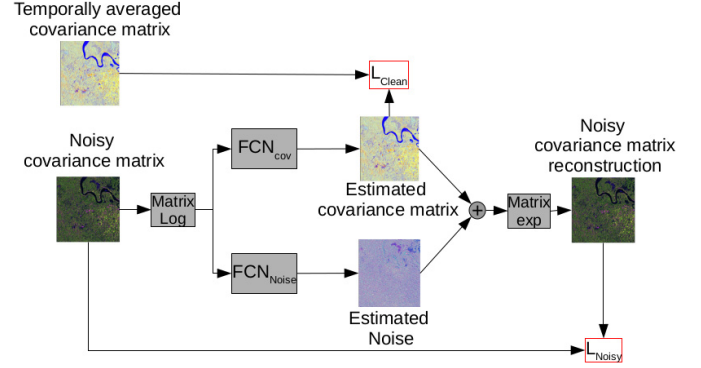

Fig. 1. Architecture of CV-deSpeckNet. The polarimetric covariance matrix in the log form follows an additive noise model. Therefore, the architecture of CV-deSpeckNet follows this model using two separate FCNs to estimate: 1) the clean covariance matrix and 2) the noise, separately. These two components are then summed up and converted to the multiplicative noise model by taking a matrix exponent to reconstruct the original noisy covariance matrix. At the test time, only the clean covariance matrix estimation part (FCN_cov) of the network is utilized.

valued deep fully convolutional network (FCN) to estimate the covariance matrix $\tilde{C}$.

B. Network Architecture

We propose a multistream complex-valued architecture named CV-deSpeckNet to estimate the covariance matrix $\tilde{C}$ and the noise $\tilde{N}$, separately (see Fig. 1). A variant for single-channel real-valued SAR intensity image despeckling was proposed in [17]. We adopted this architecture to train a robust model for learning feature representation and the underlying noise distribution in a complex-valued data, i.e., two identical FCNs estimate $\tilde{C}$ (FCN_cov) and $\tilde{N}$ (FCN_noise), separately. With those two components, we reconstruct the noisy covariance matrix $(\hat{C})$ using the assumed signal independent additive noise that results from taking the matrix logarithm of $\hat{C}$. CV-deSpeckNet is designed to rectify the limitation of deSpeckNet [17] by processing naturally complex-valued data in its native form without splitting real and imaginary components as separate channels.

Both (FCN_cov) and (FCN_noise) consist of three main building blocks: 1) complex-convolution (CV-Conv) [13]; 2) complex-activation (CReLU) [15]; and 3) complex-batch normalization (CV-BN) [13]. The architecture does not use any pooling layers to avoid upsampling layers to reconstruct the feature maps to their original sizes, as these lay additional computational burden. Instead, we maintained the sizes of feature maps in the intermediate layers and increased the depth of the network.

The deep learning objective is, therefore, formulated as

$$\arg\min_{\theta} \sum L(f_\theta(\hat{C}), C). \tag{2}$$

Here, $\hat{C}$ is the observed rank 1 covariance matrix, C is the reference covariance matrix used as a proxy for the noise-free covariance matrix, and f_θ is the deep neural network parameterized by the complex-valued parameters θ learned under the loss function L.

To train the network, we employ two types of loss functions, the sum squared error (SSE)-based L_{cov} and L_{noise}, which are combined as $L = L_{\text{cov}} + L_{\text{noise}}$.

We apply the L_{cov} loss between the reconstructed clean covariance matrix $(\tilde{C})$ and the reference temporally averaged covariance matrix (C) in the log domain.

The SSE loss function in the complex domain is identical to its real-valued counterpart given as

$$L_{\text{cov}}(\tilde{C}, C) = \mu \sum_{i=1}^{H} \sum_{j=1}^{W} \sum_{d=1}^{D} \frac{1}{2}(\tilde{C}_{ijd} - C_{ijd})^2 \quad (3)$$

where H, W, and D are the height, width, and the number of feature maps in the estimated covariance matrix, respectively, and μ is the weight assigned to the loss. Once $\tilde{C}$ and $\tilde{N}$ are reconstructed, an elementwise addition is applied, and the reconstructed noisy covariance matrix is converted to the original linear scale by taking the matrix exponent (see Fig. 1). The reconstructed noisy covariance matrix is then compared to the input covariance matrix by using another SSE-based loss L_{noise}

$$L_{\text{noise}}(\hat{\tilde{C}}, \hat{C}) = \xi \sum_{i=1}^{H} \sum_{j=1}^{W} \sum_{d=1}^{D} \frac{1}{2}(\hat{\tilde{C}}_{ijd} - \hat{C}_{ijd})^2. \quad (4)$$

Here, ξ is the weight assigned to L_{noise}.

III. DATA SETS

CV-deSpeckNet is tested using a rank 1 covariance matrix synthesized by taking the outer product of k from a dual-polarization Sentinel-1 single look complex (SLC) images acquired near the city of Jambi and the village of Tempino-ketjil, Sumatra, Indonesia. The images are acquired in the C-band in the interferometric wide swath mode (IW) in descending orbit. The images were acquired with an incidence angle of 40.02^0 and have a resolution of 3.14 m $\times$ 11.05 m. The image acquired around Jambi on May 13, 2019, and June 30, 2019, hereafter referred to as training image, was used as training data and each spanned 1000×1000 pixels. The trained model was tested on the image acquired on October 4, 2019, in the same geographical area as the training image, hereafter referred to as test image 1. In addition, an image acquired around Tempino-ketjil on May 13, 2019, hereafter referred to as test image 2, was used as the second test image. This image spanned 500×500 pixels. For synthesizing the reference labels, we used 18 images acquired from May 13, 2019, to November 21, 2019, over the same area. We used test images 1 and 2 for testing and obtaining the reported quality measurements. Test image 1 covers a mixed urban and natural scene, whereas test image 2 covers a natural environment (see Fig. 2).

IV. EXPERIMENTAL SETUP

A. Training

Since the complex arithmetic used in the building blocks of the complex-valued neural network can be simulated with real-valued arithmetic [13], the input data to the network were prepared by vectorizing the Sentinel-1 2×2 covariance
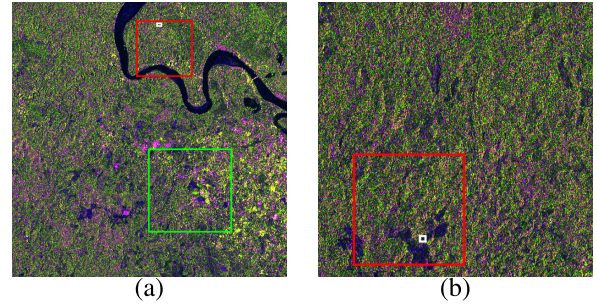

Fig. 2. Input images used to test CV-deSpeckNet. The areas in the red and green boxes were used for qualitative comparison of the methods. The areas in the small white boxes in both images were used to estimate ENL (red: C_{11}, green: C_{22}, and blue: C_{11}/C_{22}). (a) Test image 1. (b) Test image 2.

matrix into a six-channel image representing the real and imaginary parts of the upper triangular elements of the Hermitian positive semidefinite covariance matrix. The diagonal elements of the covariance matrix are real-valued intensity images, so, for mathematical convenience, we added 0_i to represent the imaginary part for these images. We also used a temporal average of 18 covariance matrices synthesized from 18 images of the same region to prepare C used as a proxy for the reference covariance matrix. We assumed polarimetric stationarity that the dominant scattering mechanism of the scene is not changing within the considered time span. Since 18 images are too few to synthesize a relatively noise-free covariance matrix, we perform additional spatial filtering using the MuLoG framework proposed in [7].

The networks were trained using the Adam optimization method. Both FCN_{cov} and FCN_{noise} consist of 17 complex-valued convolutions with 48 filters. Complex-valued Batch normalization was used for every complex-valued convolution layer except the first and prediction layers. The networks were trained for 50 epochs with a learning rate of 10^{-3} for 30 epochs and an additional 20 epochs with a rate of 10^{-4}. We set the weight (μ) of the L_{cov} to 100, and the weight (ξ) of L_{Noise} was given a value of 1. To apply this, we used a training set of 58 368 randomly selected patches of size $40 \times 40 \times 6$ representing the real and imaginary parts of the unique upper triangular elements of the covariance matrix. A minibatches of 64 samples and a weight decay factor of 5×10^{-4} were used. We trained the network using the Keras complex library [18] on the Google Colab platform using a Tesla T4 GPU.

To assess the performance of CV-deSpeckNet, we compared it with extended Lee sigma filter [19], MuLoG [7], real-valued FCN (RV-FCN) that used real-valued building blocks, and deSpeckNet [17]. RV-FCN was trained using the same architecture as FCN_{cov}. CV-deSpeckNet and deSpeckNet were trained using the same number of parameters. In both cases, unsupervised fine-tuning [17] was not applied. Extended Lee Sigma and MuLoG are both unsupervised methods that require only 1 s and 2.36 min, respectively. The training of RV-FCN required 1.3 h, whereas deSpeckNet and CV-deSpeckNet required 2.6 and 7.01 h, respectively.

B. Quality Metrics

To evaluate the performance of CV-deSpeckNet and the state-of-the-art PolSAR despeckling methods quantitatively,
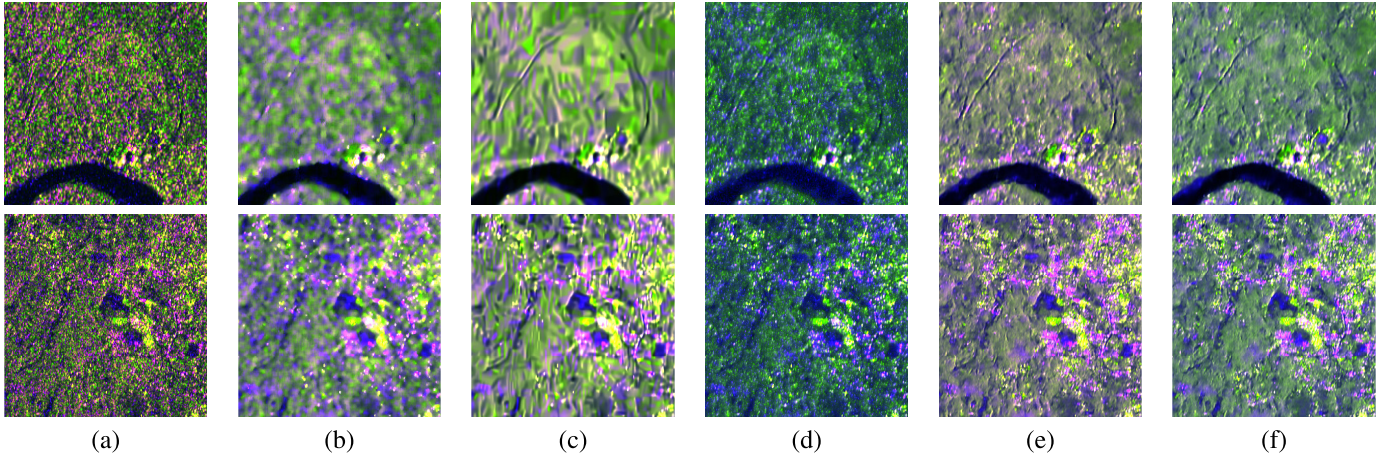
Fig. 3. Covariance matrix estimation result for a baseline method and CV-deSpeckNet for a 200×200 and 300×300 subset for test image 1 indicated on (see Fig. 2). We show the color composite (red: C_{11}, green: C_{22}, and blue: C_{11}/C_{22}) for (a) $\hat{C}$ (input), (b) extended Lee sigma, (c) MuLoG, (d) RV-FCN, (e) deSpeckNet, and (f) CV-deSpeckNet.

Fig. 4. Covariance matrix estimation result for baseline methods and CV-deSpeckNet for a 200×200 subset of test image 2. We show the color composite (red: C_{11}, green: C_{22}, and blue: C_{11}/C_{22}) for (a) $\hat{C}$ (input), (b) extended Lee sigma, (c) MuLoG, (d) RV-FCN, (e) deSpeckNet, and (f) CV-deSpeckNet.
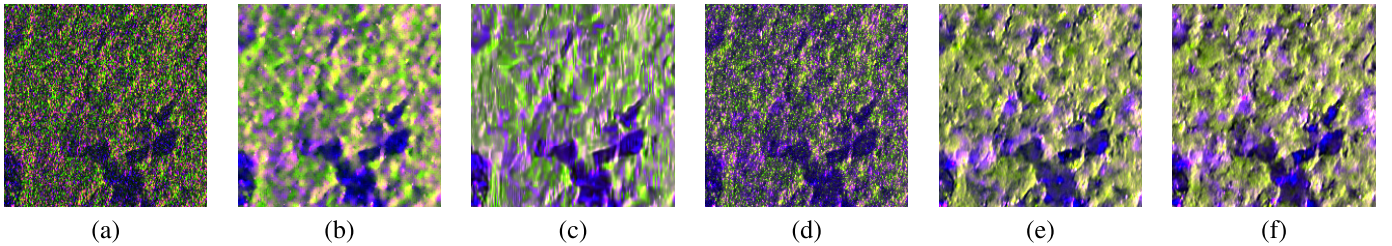
TABLE I

PSNR, SSIM, DG, ENL VALUES AVERAGED FOR THE TWO DIAGONAL ELEMENTS OF THE COVARIANCE MATRIX, AND THE $\tilde{\alpha}$, $\tilde{H}$, AND $\tilde{A}$ VALUES DERIVED FROM THE FULL COVARIANCE MATRIX. CV-DESPECKNET (TEST) REFERS TO CV-DESPECKNET FINE-TUNED ON A TEMPORALLY AVERAGED IMAGE FOR THE TEST SCENE USED AS AN UPPER BOUND

Area	Method	PSNR	SSIM	DG	ENL	$\tilde{\alpha}$	$\tilde{H}$	$\tilde{A}$
Test image 1	Lee sigma	26.43	0.76	0.11	54.61	3.47	0.062	0.058
	MuLog	26.93	0.79	0.54	46.05	2.48	0.054	0.051
	RV-FCN	20.13	0.48	-6.14	14.49	8.22	0.08	0.07
	deSpeckNet	26.82	0.78	1.49	46.99	1.75	0.041	0.038
	CV-deSpeckNet	27.06	0.79	1.05	81.46	1.75	0.04	0.03
	CV-deSpeckNet (test)	31.12	0.87	5.31	177.58	1.34	0.031	0.029
Test image 2	Lee sigma	30.93	0.73	5.09	17.45	3.70	0.06	0.05
	MuLog	32.58	0.78	9.66	12.15	3.12	0.065	0.063
	RV-FCN	21.03	0.33	-1.04	10.06	8.56	0.14	0.11
	deSpeckNet	30.92	0.72	6.72	7.40	1.28	0.03	0.028
	CV-deSpeckNet	34.49	0.82	12.73	29.08	1.25	0.027	0.025
	CV-deSpeckNet (test)	37.28	0.88	16.72	86.81	0.9	0.021	0.020

we used temporally averaged images obtained in the same areas as the test images. The quality metrics used to evaluate the performance of the compared methods in the presence of full reference label image are the peak signal to noise ratio (PSNR), structural similarity index (SSIM) [17], and despeckling gain (DG) [20]. These metrics are averaged for the diagonal elements of the covariance matrix, which are real-valued intensity images. Furthermore, to evaluate the performance of CV-deSpeckNet and compared methods, we use the absolute error of the polarimetric scattering mechanism ($\tilde{\alpha}$), entropy ($\tilde{H}$), and anisotropy ($\tilde{A}$) [16], [21] derived from the full covariance matrix.

To evaluate the despeckling ability of CV-deSpeckNet and the compared methods without reference data, we used visual

inspection as a qualitative measure and the equivalent number of looks (ENL) derived in a homogeneous region as a quantitative measure for comparison.

V. RESULTS AND DISCUSSION

A. Qualitative Assessment

In test image 1, both extended Lee sigma and MuLog resulted in a smooth output but, on close inspection, many artifacts can be observed, whereas RV-FCN failed to remove most of the speckle from homogenous regions and preserve the subtle features in the image. The filtered output still maintained the noisy appearance of the single-look covariance matrix. This was due to the insufficient number of training samples, as a progressive increase in the training set improved its performance. CV-deSpeckNet and deSpeckNet performed better than the other methods in removing speckle while preserving subtle features, such as edges and point scatterers (see Fig. 3). Since test image 1 is acquired over the training area with a different realization of speckle, the results indicate that the multistream architecture is more robust in learning underlying speckle noise.

In test image 2, both the extended Lee sigma filter and MuLog still maintained a smooth output, whereas RV-FCN still failed to remove speckle and preserve subtle features. This was expected as the image scene, and noise distribution was expected to vary from the data that it was trained on. However, CV-deSpeckNet resulted in the best output as less noise was observed in the estimated image composite and most subtle features were preserved (see Fig. 4). This clearly shows the generalization capability of multistream complex-valued

architectures. In the test regions, for all methods, supervised tuning of the model was not performed. The reference temporally averaged covariance matrix was only used to derive the quantitative quality metrics.

B. Quantitative Assessment

The potential of CV-deSpeckNet is further exemplified by the improvement of the quantitative metrics defined in Section IV-B. In test image 1, CV-deSpeckNet achieved the highest PSNR, SSIM, and ENL values compared to extended Lee sigma, MuLog, RV-FCN, and deSpeckNet (see Table I). It also achieved the lowest absolute error for ($\tilde{\alpha}$), entropy ($\tilde{H}$), and anisotropy ($\tilde{A}$) values. CV-deSpeckNet achieved the highest result in all quality metrics compared with the quantitative results in test image 2. This indicates the robust feature representation learning ability within multistream complex-valued FCNs. To establish the upper bound for test images 1 and 2, we applied supervised tuning of CV-deSpeckNet in the test images using the temporally averaged reference data. These results show that CV-deSpeckNet, ever without using supervised tuning on the test image, is able to reach comparable performance to a network tuned on a reference test image (see Table I).

VI. CONCLUSION

We have presented CV-deSpeckNet, a multistream complex-valued FCN architecture, which is able to learn a model suitable for despeckling and effective estimation of the dual-polarized covariance matrix. Our experiments on test images, obtained over different regions, confirm the robustness of CV-deSpeckNet. CV-deSpeckNet proved to be effective in estimating the covariance matrix while preserving the image quality with modest-sized training data. It was also able to learn robust feature representation that was able to adapt to a new test image. It provided better estimation results than the state-of-the-art methods and its real-valued counterpart, and a comparable performance with FCN models tuned with temporally averaged images.

ACKNOWLEDGMENT

REFERENCES

[1] J.-S. Lee, M. R. Grunes, and G. D. Grandi, "Polarimetric SAR speckle filtering and its implication for classification," *IEEE Trans. Geosci. Remote Sens.*, vol. 37, no. 5, pp. 2363–2373, Sep. 1999.

[2] J.-S. Lee and E. Pottier, *Polarimetric Radar Imaging: From Basics to Applications*. Boca Raton, FL, USA: CRC Press, 2009.

[3] J.-S. Lee, M. R. Grunes, L. Ferro-Famil, D. L. Schuler, and E. Pottier, "Scattering-model-based speckle filtering of polarimetric SAR data," *IEEE Trans. Geosci. Remote Sens.*, vol. 44, no. 1, pp. 176–187, Jan. 2006.

[4] A. G. Mullissa, V. Tolpekin, and A. Stein, "Scattering property based contextual PolSAR speckle filter," *Int. J. Appl. Earth Observ. Geoinf.*, vol. 63, pp. 78–89, Dec. 2017.

[5] J.-S. Lee and E. Pottier, *Polarimetric Radar Imaging: From Basics to Applications*. Boca Raton, FL, USA: CRC Press, 2017.

[6] C.-A. Deledalle, L. Denis, F. Tupin, A. Reigber, and M. Jäger, "NL-SAR: A unified nonlocal framework for resolution-preserving (Pol)(In)SAR denoising," *IEEE Trans. Geosci. Remote Sens.*, vol. 53, no. 4, pp. 2021–2038, 2014.

[7] C. Deledalle, L. Denis, S. Tabti, and F. Tupin, "MuLoG, or how to apply Gaussian denoisers to multi-channel SAR speckle reduction?" *IEEE Trans. Image Process.*, vol. 26, no. 9, pp. 4389–4403, Sep. 2017.

[8] G. Chierchia, D. Cozzolino, G. Poggi, and L. Verdoliva, "SAR image despeckling through convolutional neural networks," in *Proc. IEEE Int. Geosci. Remote Sens. Symp. (IGARSS)*, Jul. 2017, pp. 5438–5441.

[9] Q. Zhang, Q. Yuan, J. Li, Z. Yang, and X. Ma, "Learning a dilated residual network for SAR image despeckling," *Remote Sens.*, vol. 10, no. 2, p. 196, Jan. 2018.

[10] T. Pan, D. Peng, W. Yang, and H.-C. Li, "A filter for SAR image despeckling using pre-trained convolutional neural network model," *Remote Sens.*, vol. 11, no. 20, p. 2379, Oct. 2019.

[11] T. Nitta, "An extension of the back-propagation algorithm to complex numbers," *Neural Netw.*, vol. 10, no. 8, pp. 1391–1415, Nov. 1997.

[12] A. Hirose, *Complex-Valued Neural Networks: Advances and Applications*, vol. 18. Hoboken, NJ, USA: Wiley, 2013.

[13] C. Trabelsi *et al.*, "Deep complex networks," 2017, *arXiv:1705.09792*. [Online]. Available: http://arxiv.org/abs/1705.09792

[14] Z. Zhang, H. Wang, F. Xu, and Y.-Q. Jin, "Complex-valued convolutional neural network and its application in polarimetric SAR image classification," *IEEE Trans. Geosci. Remote Sens.*, vol. 55, no. 12, pp. 7177–7188, Dec. 2017.

[15] A. G. Mullissa, C. Persello, and A. Stein, "PolSARNet: A deep fully convolutional network for polarimetric SAR image classification," *IEEE J. Sel. Topics Appl. Earth Observ. Remote Sens.*, vol. 12, no. 12, pp. 5300–5309, Dec. 2019.

[16] A. G. Mullissa, D. Perissin, V. A. Tolpekin, and A. Stein, "Polarimetry-based distributed scatterer processing method for PSI applications," *IEEE Trans. Geosci. Remote Sens.*, vol. 56, no. 6, pp. 3371–3382, Jun. 2018.

[17] A. G. Mullissa, D. Marcos, D. Tuia, M. Herold, and J. Reiche, "DeSpeckNet: Generalizing deep learning-based SAR image despeckling," *IEEE Trans. Geosci. Remote Sens.*, early access, Dec. 17, 2020, doi: 10.1109/TGRS.2020.3042694.

[18] J. S. Dramsch, *Complex-Valued Neural Networks in Keras With Tensorflow*. Figshare, 2019. [Online]. Available: https://figshare.com/articles/Complex-Valued_Neural_Networks_in_Keras_with_Tensorflow/9783773/1, doi: 10.6084/m9.figshare.9783773.

[19] J.-S. Lee, T. L. Ainsworth, Y. Wang, and K.-S. Chen, "Polarimetric SAR speckle filtering and the extended sigma filter," *IEEE Trans. Geosci. Remote Sens.*, vol. 53, no. 3, pp. 1150–1160, Mar. 2015.

[20] G. D. Martino, M. Poderico, G. Poggi, D. Riccio, and L. Verdoliva, "Benchmarking framework for SAR despeckling," *IEEE Trans. Geosci. Remote Sens.*, vol. 52, no. 3, pp. 1596–1615, Mar. 2014.

[21] J.-S. Lee, M. R. Grunes, E. Pottier, and L. Ferro-Famil, "Unsupervised terrain classification preserving polarimetric scattering characteristics," *IEEE Trans. Geosci. Remote Sens.*, vol. 42, no. 4, pp. 722–731, Apr. 2004.